



Chinese Pharmaceutical Association  
Institute of Materia Medica, Chinese Academy of Medical Sciences

Acta Pharmaceutica Sinica B

[www.elsevier.com/locate/apsb](http://www.elsevier.com/locate/apsb)  
[www.sciencedirect.com](http://www.sciencedirect.com)



ORIGINAL ARTICLE

# Mitochondrial-targeted and ROS-responsive nanocarrier *via* nose-to-brain pathway for ischemic stroke treatment



Yan Zhang<sup>a,†</sup>, Haiyun Zhang<sup>b,†</sup>, Faquan Zhao<sup>b,†</sup>, Zhengping Jiang<sup>a</sup>,  
Yuanlu Cui<sup>b,\*</sup>, Meitong Ou<sup>a,\*</sup>, Lin Mei<sup>a,\*</sup>, Qiangsong Wang<sup>a,\*</sup>

<sup>a</sup>Tianjin Key Laboratory of Biomedical Materials, Institute of Biomedical Engineering, Chinese Academy of Medical Sciences & Peking Union Medical College, Tianjin 300192, China

<sup>b</sup>State Key Laboratory of Component-based Chinese Medicine, Research Center of Traditional Chinese Medicine, Tianjin University of Traditional Chinese Medicine, Tianjin 301617, China

Received 6 March 2023; received in revised form 12 May 2023; accepted 8 June 2023

## KEY WORDS

Ischemic stroke;  
Inflammation;  
Mitochondrial targeted;  
Multifunctional  
nanocarriers;  
Nose-to-brain pathway;  
Oxidative stress;  
Puerarin;  
ROS-Responsiveness

**Abstract** Oxidative stress injury and mitochondrial dysfunction are major obstacles to neurological functional recovery after ischemic stroke. The development of new approaches to simultaneously diminish oxidative stress and resist mitochondrial dysfunction is urgently needed. Inspired by the over-produced reactive oxygen species (ROS) at ischemic neuron mitochondria, multifunctional nanoparticles with ROS-responsiveness and mitochondrial-targeted (SPNPs) were engineered, achieving specific targeting delivery and controllable drug release at ischemic penumbra. Due to the nose-to-brain pathway, SPNPs which were encapsulated in a thermo-sensitive gel by intranasal administration were directly delivered to the ischemic penumbra bypassing the blood–brain barrier (BBB) and enhancing delivery efficiency. The potential of SPNPs for ischemic stroke treatment was systematically evaluated *in vitro* and in rat models of middle cerebral artery occlusion (MCAO). Results demonstrated the mitochondrial-targeted and protective effects of SPNPs on H<sub>2</sub>O<sub>2</sub>-induced oxidative damage in SH-SY5Y cells. *In vivo* distribution analyzed by fluorescence imaging proved the rapid and enhanced active targeting of SPNPs to the ischemic area in MCAO rats. SPNPs by intranasal administration exhibited superior therapeutic efficacy by alleviating oxidative stress, diminishing inflammation, repairing mitochondrial function, and decreasing apoptosis. This strategy provided a multifunctional delivery system for the effective

\*Corresponding authors.

E-mail addresses: [cuiyl@tju.edu.cn](mailto:cuiyl@tju.edu.cn) (Yuanlu Cui), [oumt@mail2.sysu.edu.cn](mailto:oumt@mail2.sysu.edu.cn) (Meitong Ou), [meilin@bme.pumc.edu.cn](mailto:meilin@bme.pumc.edu.cn) (Lin Mei), [wangqs@bme.cams.cn](mailto:wangqs@bme.cams.cn) (Qiangsong Wang).

<sup>†</sup>These authors made equal contributions to this work.

Peer review under responsibility of Chinese Pharmaceutical Association and Institute of Materia Medica, Chinese Academy of Medical Sciences.

<https://doi.org/10.1016/j.apsb.2023.06.011>

2211-3835 © 2023 Chinese Pharmaceutical Association and Institute of Materia Medica, Chinese Academy of Medical Sciences. Production and hosting by Elsevier B.V. This is an open access article under the CC BY-NC-ND license (<http://creativecommons.org/licenses/by-nc-nd/4.0/>).

treatment of ischemic injury, which also implies a potential application prospect for other central nervous diseases.

© 2023 Chinese Pharmaceutical Association and Institute of Materia Medica, Chinese Academy of Medical Sciences. Production and hosting by Elsevier B.V. This is an open access article under the CC BY-NC-ND license (<http://creativecommons.org/licenses/by-nc-nd/4.0/>).

## 1. Introduction

Stroke, the second leading cause of death, severely affected the daily life of survivors worldwide due to the high disability rate and the absence of clinically effective therapeutics<sup>1,2</sup>. Ischemic stroke accounted for 80% approximately of all stroke cases<sup>3</sup>. During ischemic injury, neurons around the injured area involve a series of biochemical events, such as energy failure, oxidative stress, ion imbalance, cell death (apoptosis or necrosis), and initiation of the inflammation and immune response, leading to irreversible brain damage<sup>4</sup>. Clinically, intravenous thrombolysis or mechanical thrombectomy within 4.5 h to realize recanalization to the brain is the gold standard of treatment<sup>5</sup>. This narrow therapeutic window increases the treated difficulty, and less than 10% of patients could be treated in time<sup>1,5</sup>. Additionally, reperfusion therapy to restore ischemic cerebral blood flow would cause secondary reperfusion injury induced by the production of reactive oxygen species (ROS), the concomitant mitochondrial dysfunction, and local inflammation<sup>6</sup>. Lots of preclinical studies are focusing on protecting neurons from injury for ischemia and reperfusion<sup>7,8</sup>. The lack of efficient pharmacotherapies for stroke could be rationalized by the narrow therapeutic window, complex ischemic pathological cascade, and low targeting efficiency of the drug to ischemic penumbra. There is urgently needed to develop multiple-targeted pharmacotherapy which could quickly bypass the BBB and treat complex ischemic pharmacology, to achieve improved brain penetration and therapeutic effect for ischemia injury.

Although the studies showed that the occurrence of ischemic stroke could destroy the permeability, the BBB remained the main barrier for therapeutic agents to the brain<sup>9</sup>. Innovative strategies that directly deliver therapeutic agents to the brain crossing the BBB are urgently needed to be developed. Invasive intracerebral administration could quickly deliver drugs to the brain, but it was challenged for its complex operation<sup>10</sup>. In recent years, noninvasive intranasal administration, allowing drugs directly reach the ischemic penumbra *via* the nose-to-brain pathway, has attracted attention in the treatment of brain diseases<sup>11,12</sup>. Intranasal administration could bypass the BBB barrier and directly deliver drugs to the penumbra within minutes along both the olfactory and trigeminal nerves<sup>13,14</sup>. FDA has approved some intranasal drugs such as Spravato and VALTOCO to treat depression and epilepsy, respectively. In light of these advantages, the intranasal administration of therapeutics should be a promising strategy to achieve fast brain accumulation by direct nose-to-brain delivery.

Recently, advances in nanocarrier-based drug delivery systems with multifunctional properties have enabled innovative and targeted treatment of brain diseases<sup>15,16</sup>. Oxidative stress and mitochondrial dysfunction are two major obstacles to neurological functional recovery after ischemic stroke<sup>17</sup>. Thus, the development of a drug delivery system to simultaneously intervene in oxidative stress and mitochondrial dysfunction may achieve improved treatment of ischemic stroke. Growing attention has

been paid to integrated multifunctional nanoparticles, especially those with targeting ability and microenvironment-responsive<sup>18,19</sup>. Aiming at the oxidative ischemic environment and therapeutic targets of stroke, ROS responsive nanocarrier with mitochondrial-targeted has been introduced as an efficient platform<sup>20</sup>. Previous studies have reported a series of ROS-responsive structures such as aryl-boronate esters/acid, sulfides, thioethers, thioketal linkage, selenium, etc.<sup>21,22</sup>. Among these sites, the thioketal linker, which is sensitive to H<sub>2</sub>O<sub>2</sub> and O<sub>2</sub><sup>-</sup>, is an attractive candidate to construct ROS-responsive nanoparticles<sup>23</sup>. Another concern for designing nanocarrier is the direct delivery to mitochondria, which possess abundant ROS to trigger selective cleavage. Bendavia (SS-31) as a member of the Szeto-Schiller peptide family is identified as a mitochondrial-targeting peptide that could selectively partition to the inner mitochondrial membrane without depending on the membrane potential<sup>24</sup>. Additionally, the SS-31 demonstrates an anti-oxidative capacity by reducing mitochondrial ROS production and inhibiting mitochondrial permeability transition, which is beneficial to exert protection against ischemic reperfusion damage. It has been reported that the SS-31 peptide-modified quercetin could realize mitochondrial targeting of damaged neurons to achieve neuron protection in model animals<sup>25</sup>. A multifunctional SS31-modified nano-micelles achieved the repairment of mitochondrial function and alleviation of hierarchically oxidative to reduce myocardial ischemia-reperfusion injury<sup>26</sup>. Therefore, nanocarriers with thioketal linker crosslink and SS-31 decoration could exert the functions as ROS-responsiveness, mitochondrial-targeted, and antioxidation, achieving neuron protection for ischemic stroke.

Natural products from herbal medicines have been paid more attention owing to their vast structural diversity with biological relevance, which is widely approved by FDA as small molecule drugs and used due to their wide application, high safety, and minimum side effects<sup>27</sup>. Puerarin (PU), the major bioactive ingredient of the *Pueraria lobata* (Willd.) Ohwi, has been demonstrated multiple pharmacological properties, including vasodilation, anti-oxidation, anti-inflammation, neuroprotection, etc. Clinically, puerarin injection has been approved in the treatment of myocardial ischemia in China<sup>28</sup> by attenuating the expression of the inflammatory mediators, improving energy metabolism, reducing oxidative stress, and accelerating cardiac angiogenesis. In addition, puerarin could also alleviate mitochondrial dysfunction by inhibiting mitophagy-mediated reduction in mitochondrial mass, maintaining mitochondrial membrane potential, preventing Cytochrome C release, and reducing caspase activity. However, PU displayed limited application in brain disease due to its low solubility, short elimination half-life, and low bioavailability<sup>29</sup>. Thus, encapsulating PU in a multifunctional delivery system would be an optimal strategy to exert its multiple pharmacological activities with targeted delivery.

Herein, we fabricated the nanocarriers (SPNPs) with diverse functions as mitochondrial-targeted, ROS-responsive release, and

anti-oxidative stress to achieve the promising therapeutic effect for ischemia-reperfusion injury by regulating the oxidative microenvironment and mitochondria function (Fig. 1). The thioether crosslinked skeleton of SPNPs was ruptured in response to the microenvironment ROS, exerting the activity to eliminate ROS and achieving the controlled release of loaded PU. The decoration of the SS-31 peptide achieved the mitochondrial target. Then SPNPs were encapsulated into a thermo-sensitive hydrogel for intranasal administration. By direct nose-to-brain delivery, the SPNPs were fast accumulated at ischemic penumbra, and then targeted to mitochondria with the favor of SS-31. Triggered by the abundant ROS at mitochondria, ROS-responsive skeleton in SPNPs and SS-31 could deplete ROS to reduce oxidative stress and cascade inflammatory response. Meanwhile, the ROS-responsive release of PU could repair mitochondrial function by maintaining ATP metabolism and membrane function to inhibit the cytochrome C-mediated apoptosis. In brief, the multifunctional nanoparticles integrated ROS-responsiveness, mitochondrial target, and antioxidation, distributing great potential to treat ischemia-reperfusion injury after stroke.

## 2. Materials and methods

### 2.1. Fabrication and characterization of ROS-responsive nanoparticles

The ROS-responsive nanoparticles were prepared in a water-in-oil (W/O) emulsion-crosslinking approach with Polysorbate 85 as a surfactant and H<sub>2</sub>O<sub>2</sub>-sensitive PDAA as a crosslinker.

### 2.2. Mitochondrial targeting

Accumulation of nanoparticles in mitochondrial fractions was assessed by confocal laser scanning microscope). After co-incubation with nanoparticles, the SH-SY5Y cells were stained by Hoechst 33,342 and Mito-tracker Red CMXRos to identify the nucleus and mitochondrial, respectively.

### 2.3. *In vitro* neuroprotective effects in the oxidative stress (OS) cell model

SH-SY5Y cells treated with H<sub>2</sub>O<sub>2</sub> to establish the OS model. Then the SPNPs solution was added, and the cell viability was determined with a CCK8 assay. To compare the neuroprotective effects between different therapeutic agents, the cells were co-incubated with kinds of nanoparticles solution, and cell viability were determined with CCK8 assay and LDH cytotoxicity assay, respectively.

### 2.4. Protection against intracellular ROS and mitochondrial membrane potential

The depletion of the intracellular ROS in the OS cell model was monitored with a 2',7'-Dichlorodihydrofluorescein diacetate (DCFH-DA) assay. The OS model SH-SY5Y cells were incubated with kinds of therapeutic agents and subsequently stained with DCFH-DA for 30 min. Then intracellular DCFH fluorescence intensity was analyzed by flow cytometry.

To monitor the protection of SPNPs against mitochondrial membrane potential, the OS model cells, treated with therapeutic

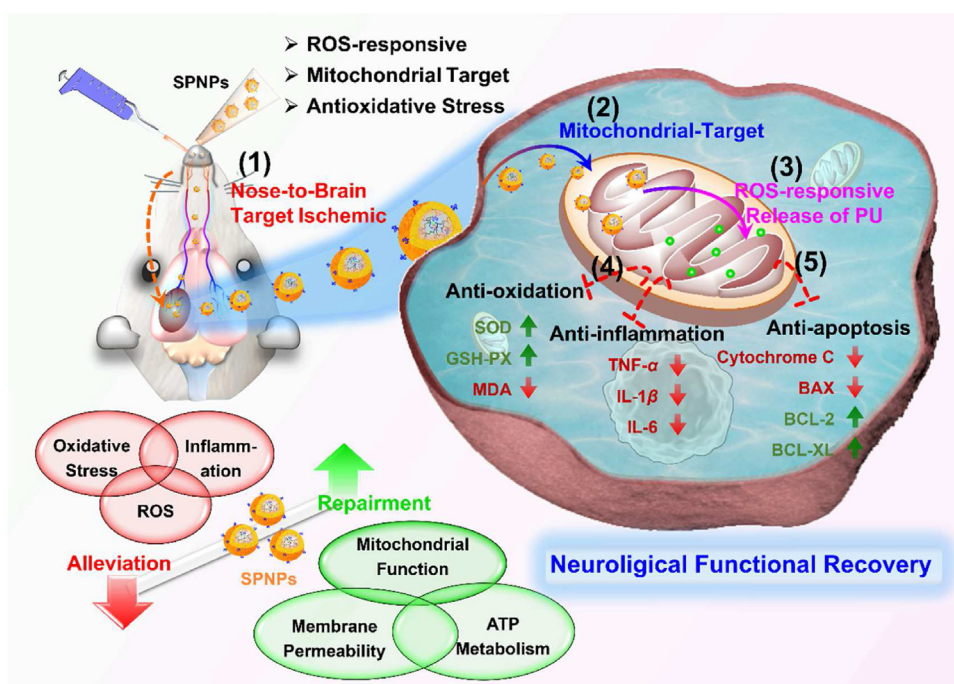


**Figure 1** Schematic illustration of targeted treatment of ischemic stroke by ROS-responsive nanoparticles loaded with PU and decorated with SS31. (1) Intranasal administration of SPNPs hydrogels to achieve the direct target to ischemic penumbra by nose-to-brain pathway. (2) The intracellular transport and mitochondrial-targeted delivery of SPNPs by the conjugated SS-31 peptide. (3) Cleavage of the ROS responsive linker to release loaded PU. (4) Depletion of ROS by released PU, ROS-responsive skeleton in SPNPs and SS-31 to alleviate oxidative stress and cascaded inflammation. (5) The rescued mitochondrial function with blockade of cytochrome *c* release and inhibition of cell apoptosis.

agents were incubated with mitochondrial JC-1 dye, and visualized on a CLSM. During observation.

### 2.5. Animals

Male Wistar rats (6–8 weeks old, 260–280 g) were purchased from the Vital River Laboratory Animal Technology Company (Beijing, China) and kept under SPF conditions for 3 days before the study, with free access to standard food and water. All of the studies comply with the Principles of Care and Use of Laboratory Animals set by the Institutional Animal Care and Use Committee of Tianjin University of Traditional Chinese Medicine (TCM-LACE2021226).

### 2.6. *In vivo* distribution of nanoparticles

The experiment of *in vivo* distribution was as follows. 5 min after reperfusion, rats were intranasal (I.N.) administration with thermo-sensitive CRNPs-gels or SCRNP-gels, respectively. At a preset time point, the rats were sacrificed and the main organs (brain, heart, liver, spleen, lung, and kidney) were collected and imaged by IVIS. Semiquantitative analysis was performed by region of interest (ROI) analysis.

### 2.7. *In vivo* anti-ischemic stroke efficacy

The sham-operated group was used as the negative control. To assess the optimized SPNPs dosage, the middle cerebral artery occlusion (MCAO) rats were weighed and randomly divided into different groups, three groups were intranasally administrated with SPNPs-gels. To evaluate the therapeutic efficacy of different therapeutic nanoparticles, the MCAO rats were intranasally administrated with different thermo-sensitive gels, which contained PU, PNPs, SPNPs, or SNPs, respectively. The positive group was intravenously injected with Edaravone, and the negative one was intranasally administrated with saline gels. The therapeutic agents were administrated every day for 3 days, and the therapeutic efficacy was evaluated by measurement of neurological scores, TTC (2,3,5-triphenyl tetrazolium chloride) staining of the brain, and brain water content.

### 2.8. Investigation of the mechanism of SPNPs against ischemic stroke

The alleviation of oxidative stress in the ischemic brain hemisphere was evaluated by measuring the activities of oxidative stress indicators such as superoxide dismutase (SOD), malondialdehyde (MDA), and glutathione peroxidase (GSH-PX) in the homogenate of the isolated ischemic brain. The inflammatory cytokines, tumor necrosis factor (TNF)- $\alpha$ , interleukin 6 (IL-6), and interleukin 1 $\beta$  (IL-1 $\beta$ ), were also evaluated by ELISA kit. To assess the mitochondrial function, the activities of ATP, Na<sup>+</sup>-K<sup>+</sup>-ATPase, and Ca<sup>2+</sup>-Mg<sup>2+</sup>-ATPase were analyzed. And the mitochondrial morphology was observed by TEM.

### 2.9. Statistical analysis

All data in this study were expressed as mean  $\pm$  SD *in vitro* or mean  $\pm$  SE *in vivo*. Comparisons between individual points were evaluated by one-way analysis of variance including Turkey and Scheffe's means comparison using Origin software. *P* values less than 0.05 is considered statistically significant.

## 3. Results and discussion

### 3.1. Characterization of ROS-responsive nanoparticles

A nanocarrier with diverse pharmacological activities such as antioxidation, mitochondrial-targeted, and ROS responsiveness was promising for ischemic stroke treatment. Herein, a multi-functional nanoparticle with ROS responsiveness, antioxidation, and mitochondrial target, was fabricated, which was crosslinked *via* H<sub>2</sub>O<sub>2</sub>-sensitive crosslinker PDAA (Fig. 2A). To realize the mitochondrial targeting, the SS-31 peptide as the target was conjugated onto chitosan to form CS-*g*-SS31 (Supporting Information Fig. S1), and the grafting efficiency was quantified by HPLC *via* assessing the unconjugated peptide. Results demonstrated that the conjugation degree of SS31 was  $39.43 \pm 1.68\%$  (*w/w*). Then the CS-*g*-SS31 was characterized by Fourier transform infrared spectroscopy (FT-IR) (Supporting Information Fig. S2) and circular dichroism (CD) (Supporting Information Fig. S3). Compared with the spectra of CS or SS-31, the characteristic peaks of these two components were displayed in the mixture sample, while a new characteristic peak at  $1704.1 \text{ cm}^{-1}$  was observed in CS-*g*-SS31, referring to the successful conjugation (Fig. S2). The CD spectra (Fig. S3) further confirmed this result. The characteristic peaks referred to SS-31 peptide in CS-*g*-SS31 were missed due to the conjugation of SS-31 peptide restricting its secondary conformation in solution, which was certified by analyzing the secondary structure of CD spectra according to Yang's Reference.

Then the multi-functional nanoparticles were fabricated by a water-in-oil approach, and the hydrophobic core could be used to encapsulate the hydrophobic therapeutic drug (PU) by hydrophobic force, increasing its solubility in nanoparticles. Herein, the size and polydispersity of blank and drug-loaded ROS-responsive nanoparticles were determined (Supporting Information Table S1). Compared with blank nanoparticles (NPs), the diameters of PU encapsulated nanoparticles (PNPs) and SS-31 peptide decorated nanoparticles with mitochondrial targeting (SNPs) were increased little, and the PU encapsulated and SS-31 peptide decorated nanoparticles (SPNPs) with dual functions as mitochondrial targeting and ROS-responsive demonstrated the largest size diameter. The average hydrodynamic diameters (Fig. 2B) of PNPs and SPNPs were  $24.75 \pm 0.81$  and  $32.82 \pm 1.32$  nm, respectively. TEM images (Fig. 2C) revealed that the PNPs and SPNPs displayed spherical structures. The zeta potential of PNPs and SPNPs was  $+ (13.5 \pm 2.3)$  and  $+ (16.0 \pm 3.1)$  mV, respectively. The PU loading capacity of PNPs and SPNPs was  $2.78 \pm 0.15$  or  $2.68 \pm 0.53\%$  (*w/w*), respectively. Then the nanoparticles were characterized by FT-IR (Supporting Information Fig. S4). The newly generated peak at  $1740 \text{ cm}^{-1}$ , referred to as C=O stretching vibration of ester, indicated the crosslinking structure in nanoparticles by PDAA linker. And the observation of PU characteristic peaks at  $1200\text{--}1300 \text{ cm}^{-1}$  demonstrated the successful encapsulation of PU. Then the samples were further detected by DSC (Supporting Information Fig. S5). Chitosan demonstrated the characterized peak assigned to the degradation of chitosan at  $310 \text{ }^\circ\text{C}$ , and PU showed the crystal melting peak at about  $207.11 \text{ }^\circ\text{C}$ . While, these characteristic peaks disappeared in the PNPs, SNPs, and SPNPs, indicating that a new phase was formed in the nanoparticles.

Owing to the PDAA linker in the skeleton, the nanoparticles responded to the oxidative environment. Then ROS-responsive release, the size changes, and free radical scavenging efficacy were recorded to evaluate the antioxidation. The release profile of SPNPs was assessed in a medium with or without  $500 \text{ } \mu\text{mol/L}$

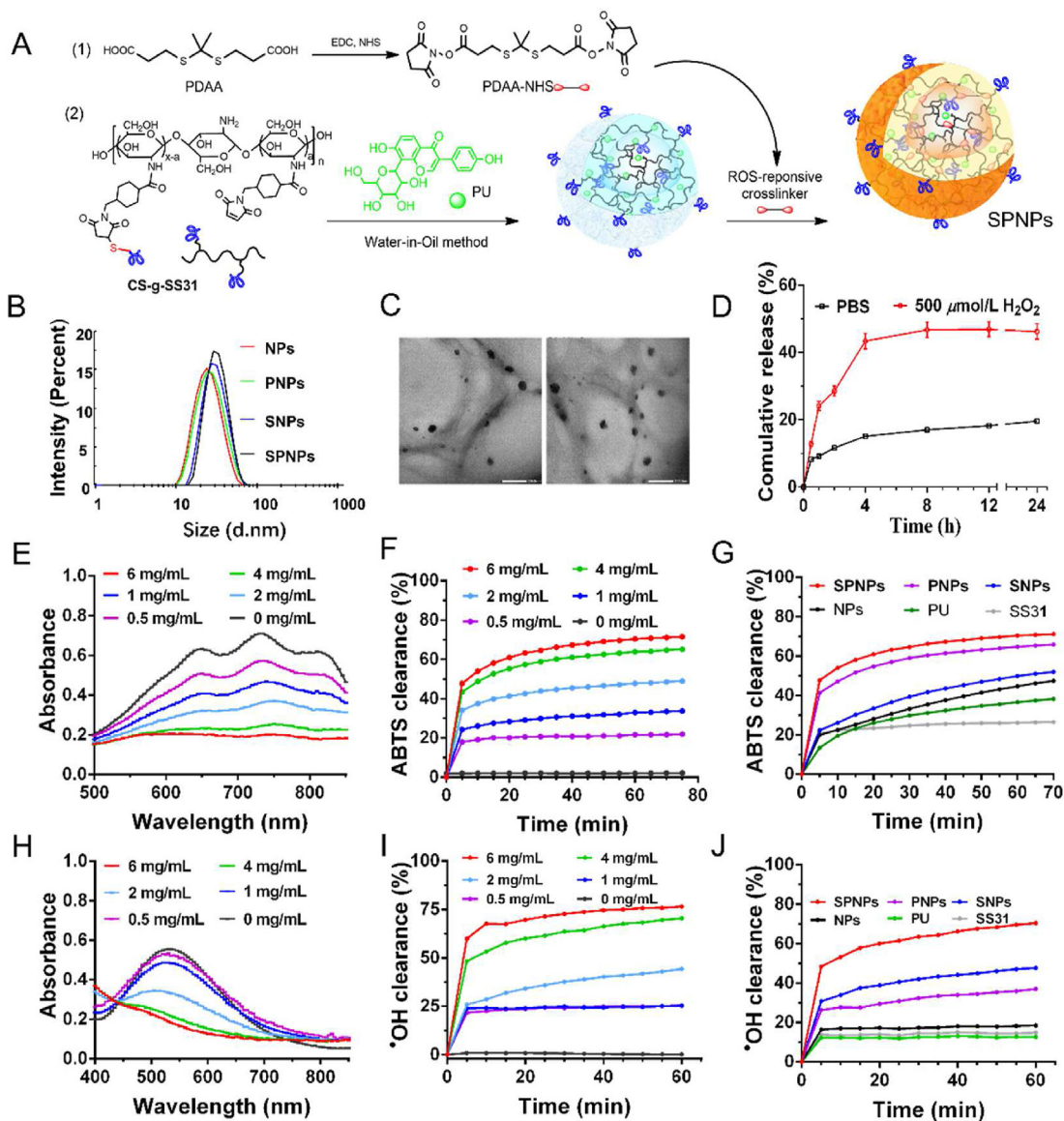


**Figure 2** The synthesis and characterization of nanoparticles. (A) Schematic illustration of the fabrication of ROS-responsive and mitochondria-targeted nanoparticles with PU encapsulation. (B) Hydrate particle size and (C) TEM images of different ROS-responsive nanoparticles, scale bar = 200 nm. (D) *In vitro* release profiles of PU from SPNPs in PBS or medium with 500  $\mu\text{mol/L}$   $\text{H}_2\text{O}_2$ . (E) UV–Vis absorption spectra of SPNPs with ABTS solution with different concentrations for 60 min. (F) The scavenging rate of ABTS free radicals by different concentrations of SPNPs. (G) The scavenging rate of ABTS free radicals by PU, SS-31 peptide, NPs, SNPs, PNPs, and SPNPs. (H) UV–Vis absorption spectra of SPNPs with Fenton solution with different concentrations. (I) The scavenging rate of hydroxyl radicals by different concentrations of SPNPs for 60 min. (J) The scavenging rate of hydroxyl radicals by PU, SS-31 peptide, NPs, SNPs, PNPs, and SPNPs. (NPs, blank nanoparticle; PNPs, PU-loaded nanoparticles; SPNPs, PU-loaded and SS-31-decorated nanoparticles; SNPs, SS-31-decorated nanoparticles).

$\text{H}_2\text{O}_2$  (Fig. 2D) to evaluate the oxidation effect on the release rate of SPNPs. The data illustrated that the cumulative release of PU was about 48% from SPNPs in the presence of  $\text{H}_2\text{O}_2$ . While only about 18% PU is released in the absence of  $\text{H}_2\text{O}_2$ . This indicated that the PU release behavior was  $\text{H}_2\text{O}_2$ -dependent, and the accelerated release profile happened in the ROS environment. The size changes of nanoparticles in the ROS environment (Fig. S6) were recorded by DLS. Incubating with an  $\text{H}_2\text{O}_2$  medium, the structure of nanoparticles was partially destroyed, and larger particles appeared. Then the ROS-scavenging ability of nanoparticles was further inspected by 2,2'-azinobis-(3-ethyl benzo thiazoline-6-sulfonate) (ABTS) assay and Fenton reaction. ABTS

assay was used to evaluate the ability of nanoparticles to deplete peroxides, and the Fenton reaction with salicylic acid was used to test the elimination against hydroxyl radical ( $\cdot\text{OH}$ ). The radical scavenging ability was time-dependent and concentration-dependent (Fig. 2E–J, and Supporting Information Figs. S7 and S8). Compared with free PU and SS-31 peptide, the nanoparticle's skeleton demonstrated a higher ROS elimination ability. The rapid clearance of ABTS and HO radicals was observed in the first 5 min in nanoparticle groups, indicating the instantaneous anti-oxidation property of the thioketone crosslinked skeleton. While, the released PU and SS-31 peptide demonstrated the sustained ROS-scavenging ability, and a stepwise increase of radical

clearance was exhibited. Compared with the first 5 min, a slower radical clearance rate was observed in the following 60 min. The oxidative stress should be relieved in the ensemble SPNPs, including the thioketal crosslinked skeleton, loaded PU, and decorated SS-31 peptide.

### 3.2. *In vitro* neuroprotection of SPNPs on the oxidative stress cell model

To evaluate the therapeutic potential of SPNPs on neuron survival and function during ischemic stroke, the *in vitro* oxidative stress (OS) cell model was established with SH-SY5Y cells (Supporting Information Fig. S9)<sup>30</sup>. As known, mitochondrial dysfunction and high level of neurotoxic ROS play a significant role in cell injury and death after ischemic stroke. Thus, the functions of SPNPs to protect mitochondrial function and alleviate oxidative stress were beneficial for neuroprotection. Firstly, to observe the uptake and mitochondrial-targeted nanoparticles, the fluorescent Cou-6 was loaded into nanoparticles (Table S1). Flow cytometry data (Supporting Information Fig. S10) showed that the increase in cellular Cou-6 fluorescence intensity was time-dependent. Compared with CNPs, the intracellular accumulation of SCNPs was faster. The intracellular fluorescence intensity of SCNPs was approximately 3-fold higher than that of CNPs within 12 h incubation. Then, the mitochondrial-targeted was determined by staining cells with Mitotracker Red (Fig. 3A and Supporting Information Fig. S11). The overlay of green (nanoparticles) and red (mitochondria) fluorescence could be observed. Colocalization analysis showed that the colocalization coefficients of CNPs and SCNPs nanoparticles in mitochondria were 0.276 and 0.382, respectively. This data indicated that SCNPs were more likely to target mitochondria due to the conjugation of SS-31 peptides.

To evaluate the mitochondrial function rescued by SPNPs, the mitochondrial membrane potential was detected by JC-1 staining (Fig. 3B and C). In healthy cells, mitochondria proposed a high membrane potential with the aggregation of JC-1 to emit red fluorescence. Upon injury, the decrease of membrane potential induced the monomers of JC-1 to emit green fluorescence. The ratio of red fluorescence to green fluorescence could be set as an indicator to detect mitochondrial membrane potential, indicating the permeability of the mitochondrial membrane. Compared to normal cells, the increased green fluorescence could be observed in OS model cells with a stimulated ischemic oxidative stress environment. While, cells treated with therapeutic agents (SPNPs, PNPs, or PU) demonstrated the remedy for the undesired fluorescence change, with the decrease of green and increase of red fluorescence (Fig. 3B). Measurement of the fluorescence (Fig. 3C) significantly demonstrated the change of green to red fluorescence. Comparison among different groups illustrated that SPNPs treatment possessed the highest red-to-green fluorescence ratio, indicating that the SPNPs could highly maintain the mitochondrial function.

Then the antioxidative effect of SPNPs was assessed with 2,7-dichloro-dichlorofluorescein diacetate (DCFH-DA) staining (Fig. 3D and E). Enhanced green fluorescence intensity revealed the excessive generation of ROS in OS model cells, consistent with the acute oxidative stress after ischemia. While, the increased intracellular fluorescence by OS modeling was significantly suppressed in the cells treated with nanoparticles, and the most significant declination was observed by SPNPs treatment, indicating the optimal antioxidative protection of SPNPs on cells. Finally, the protection of SPNPs on OS model cells was evaluated with CCK8 and LDH release assay. Data (Fig. 3F) showed that cell death

induced by oxidative stress was significantly rescued, and the neuroprotective efficacy of SPNPs was dose-dependent.

According to the CCK8 and LDH release assay data (Fig. 3G and H), SPNPs demonstrated the highest cell viability. With the data of radical scavenging efficiency, the SPNPs could efficiently deplete the intracellular ROS to alleviate oxidative stress, rescuing cell viability. Collectively, these data provided that the SPNPs could first accumulate in model cells and targeted transport to the mitochondria. Subsequently, the ROS-responsive linker PDAA was cleaved by higher cellular ROS levels to release the encapsulated PU. Furthermore, the synergy effect of released PU and SS-31 could reduce the acute oxidative stress and defense the mitochondria function, exerting protection on OS model cells.

### 3.3. Preparation and characterization of *in situ* gel

The gel properties as gelation temperature and time affected the thermo-sensitive nasal gel efficiency in preventing nasal runoffs and prolonging the residence time<sup>31</sup>. A feasible gel formation could overcome the rapid nasal mucociliary clearance to improve topical drug bioavailability. Firstly, the gelation temperature was evaluated by rheology analysis. The  $G'$  value increased with temperature, which confirmed the transformation from a liquid state to a semi-solid structure (Supporting Information Fig. S12). The point where  $G'$  and  $G''$  crossed was set as the  $T_{\text{sol-gel}}$  value, and all samples displayed the gel temperature within the reported physiological temperature in the nasal cavity (32–35 °C)<sup>32</sup>. The gelation temperature was increased with the increase of Poloxamer 188 (P188) and the decrease of Poloxamer 407 (P407). Then the gelation time was further determined by the inverted tube method. Images (Supporting Information Fig. S13) visually showed the fluidity of the different composition gels at 29 °C, and similar results were obtained as rheology analysis. Thus, the optimized P407 and P188 formulation was 18% and 2% by considering gelling time and actual operation time, achieving a suitable gelation temperature for the thermos-reversible *in situ* nasal gel. In the following experiments, all the gels within intranasal administration were prepared with this optimized condition.

Pictures (Fig. 4A) demonstrated different hydrogels containing different therapeutic agents, and no significant liquid flow was observed, indicating the formation of stable hydrogels. Then the *in vitro* release of nanoparticles or drugs from the gels was determined with Rb-labeling nanoparticles (CRNPs and SCRNPs). Meanwhile, fluorescent Rb was used to simulate the release of free drugs in the hydrogel. A fast release of the free drug could be observed (Fig. 4B), and all of Rb was released in 5 h. While, nanoparticles were sustained released from gels, accompanied by hydrogel corrosion. After 12 h, about 80% of Rb-labelled nanoparticles could be detected and released into the medium. Of note, the Rb-hydrogel demonstrated a faster degradation rate than the nanoparticles-gels. The Rb-gels were denuded in 8 h (Fig. 4B), while, about 65% of the nanoparticles-gels remained in 8 h (Fig. 4C and D). This is ascribed that chitosan polysaccharide, which constitutes nanoparticles, participated in the three-dimensional network structure of the gel, increasing the strength and stability of the gel. It was further studied the release profile of PU from the SPNPs-hydrogels, and data also illustrated the sustained release behavior, followed by the corrosion of gels (Fig. 4E). To understand the release mechanism of nanoparticles from *in situ* gel, data were analyzed with origin software, and data demonstrated that the suitable model for nanoparticles from the gel was the Weibull model with the  $R^2$  was 0.991.

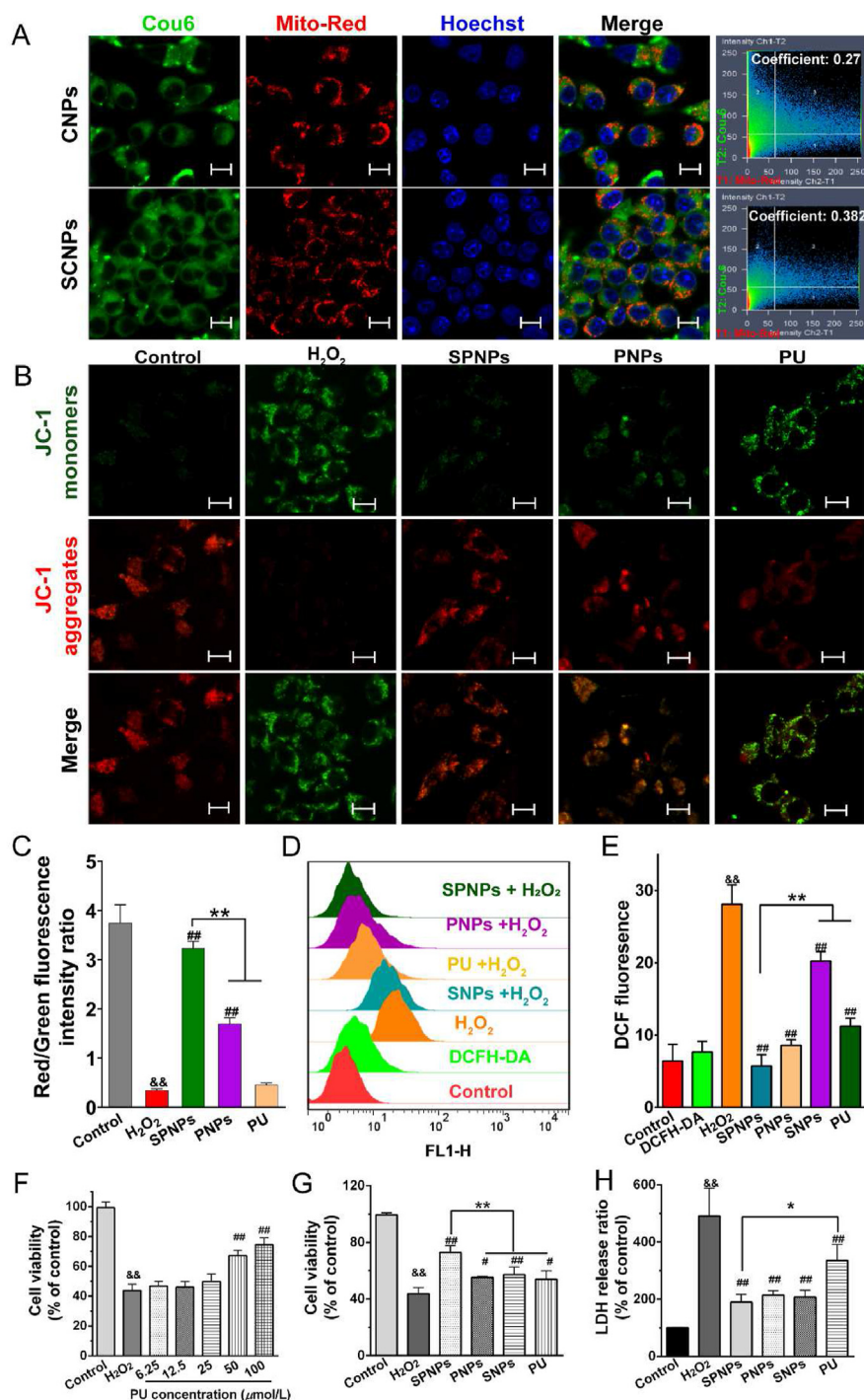


**Figure 3** *In vitro* neuroprotection on SH-SY5Y cells simulated oxidative stress environment after acute ischemic stroke. (A) Representative fluorescence images and colocalization analysis of cells with CNPs and SCNPs treatment. (B) Representative fluorescence images and (C) quantitative analysis of JC-1 staining in SH-SY5Y OS model cells treated with different therapeutic agents. (D) Flow cytometry images and (E) quantitative analysis of DCFH-DA staining to monitor intracellular ROS level. (F) Cell viability of OS model SH-SY5Y cells treated with SPNPs with different PU concentrations. (G) Cell viability and (H) LDH release ratio of SH-SY5Y OS model cells treated with different therapeutic agents. Scale bar = 10 μm. Data are presented as mean ± SD ( $n = 3$ ). && $P < 0.01$  vs. control group; # $P < 0.05$  or ### $P < 0.01$  vs. H<sub>2</sub>O<sub>2</sub> group; \* $P < 0.05$  or \*\* $P < 0.01$  vs. SPNPs group.

### 3.4. *Ex vivo* biodistribution

To assess the active targeting capability of the nanoparticles to the ischemic site, the *in vivo* distribution of Rb-labeled nanoparticles

was established in the MCAO model rat, using Cou-6 as model drugs. Firstly, the fluorescence images of the CRNPs and SCRNPs were recorded to differentiate fluorescent signals from the drug (Cou-6) and nanoparticles (Rb). Images (Supporting Information

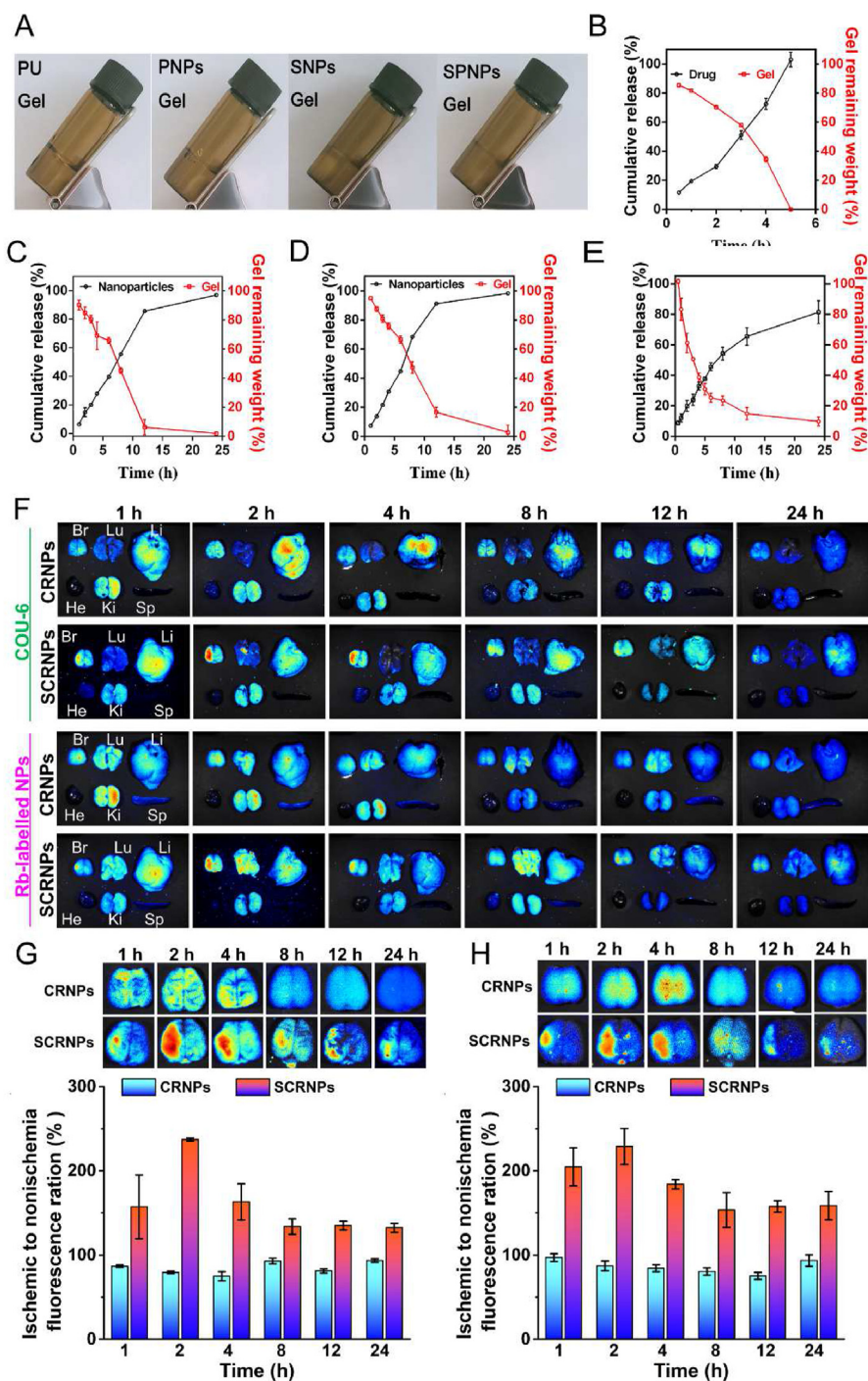


**Figure 4** Characterization of thermo-sensitive gels containing different therapeutic agents and *ex vivo* biodistribution of therapeutic nanoparticles. (A) Images of hydrogels containing different therapeutic agents by inverted vial method. Cumulative release curve of Rb signals and gel weight remaining curve of hydrogels containing (B) Rb, (C) RPNs, and (D) SRNPs at 32 °C. (E) Cumulative release curve of PU and gel weight remaining curve from SPNPs-hydrogels at 32 °C. (F) *Ex vivo* fluorescence images of vital organs (Br: Brain, Lu: Lung, He: Heart, Li: Liver, Ki: Kidney, Sp: Spleen). *Ex vivo* fluorescence images (Left ischemic hemisphere; Right normal hemisphere) and relative fluorescent analysis of signals from (G) Cou-6 and (H) Rb-labelled nanoparticles in the brain, respectively. Data are presented as mean  $\pm$  SD ( $n = 3$ ).

Fig. S14) could separate Cou-6 (model drug) and Rb (nanoparticles) successfully and provide valuable operational data for imaging *ex vivo*. The organs and brains were collected, and the *ex vivo* fluorescence images were conducted (Fig. 4 F, Supporting

Information Figs. S15 and S16). Compared with rats administrated with free Cou6 (Fig. S15), more intense fluorescence in the brain could be observed in the rats administrated with nanoparticles (CRNPs and SCRNP). Fluorescence images (Fig. 4F

and Fig. S15) demonstrated that fluorescence signals in the brain could be observed at 1 h and peaked at 2 h. Then the fluorescence intensity exhibited a gradual decline after 2 h but was still clearly visible in the brain at 24 h post-administration. Notably, compared with CRNPs, the SCRNP group had a prominent accumulation in the ischemic left brain at various times. Meanwhile, fluorescence signals from Cou-6 or Rb-labelled nanoparticles demonstrated a similar *in vivo* distribution. In the *ex vivo* fluorescence images (Fig. 4 G and H) of the ischemic brains, the accumulative fluorescence intensity of SCRNP in the left ischemic hemisphere was higher than that of the nonischemic brain, while the fluorescence signal distribution of CRNPs was uniform in the whole brain. Furthermore, the fluorescence ratio of the ischemic hemisphere to the nonischemic hemisphere in SCRNP was higher than that of CRNPs (Fig. 4 G and H), indicating the selective distribution of the active targeting ability of SCRNP to the ischemic site through SS-31 modification. In addition, both Cou-6 referred to as a model encapsulated drug, and Rb indicated as nanoparticles fluorescence signals demonstrated a similar distribution, indicating the successful targeted delivery of the drug to the ischemic site by the ROS-responsive nanoparticles.

### 3.5. *In vivo* anti-ischemic stroke efficacy

The anti-ischemic stroke effect was determined with an established MCAO model, and the protocol was illustrated (Fig. 5A). Firstly, the optimized PU dosage was evaluated with intranasal administration of SPNPs-gel, and the infarct volume was assessed to perform the optimal PU dosage. Compared with MCAO model groups, data demonstrated (Supporting Information Fig. S17) that the infarct area (white) was decreased with PU dosage. The group that accepted the middle PU dosage showed a similar infarct volume as the positive Edaravone group, while the lowest infarct area was displayed in the rats with 0.5 mg/kg PU in the SPNPs-gel group. In the following experiments, the PU dosage was 0.5 mg/kg to evaluate the anti-ischemic stroke efficacy of different kinds of therapeutic agents, and the infarct area, neuro score, and cerebral water content were accessed 3 days after the ischemic perfusion to investigate the neuroprotection.

The infarct area with TTC staining (Fig. 5B and C) reached 60% of the total brain tissue after MCAO, the group treated with free PU-gel demonstrated no reduction in infarct volume, while the decrease of brain tissue damage was significantly observed in

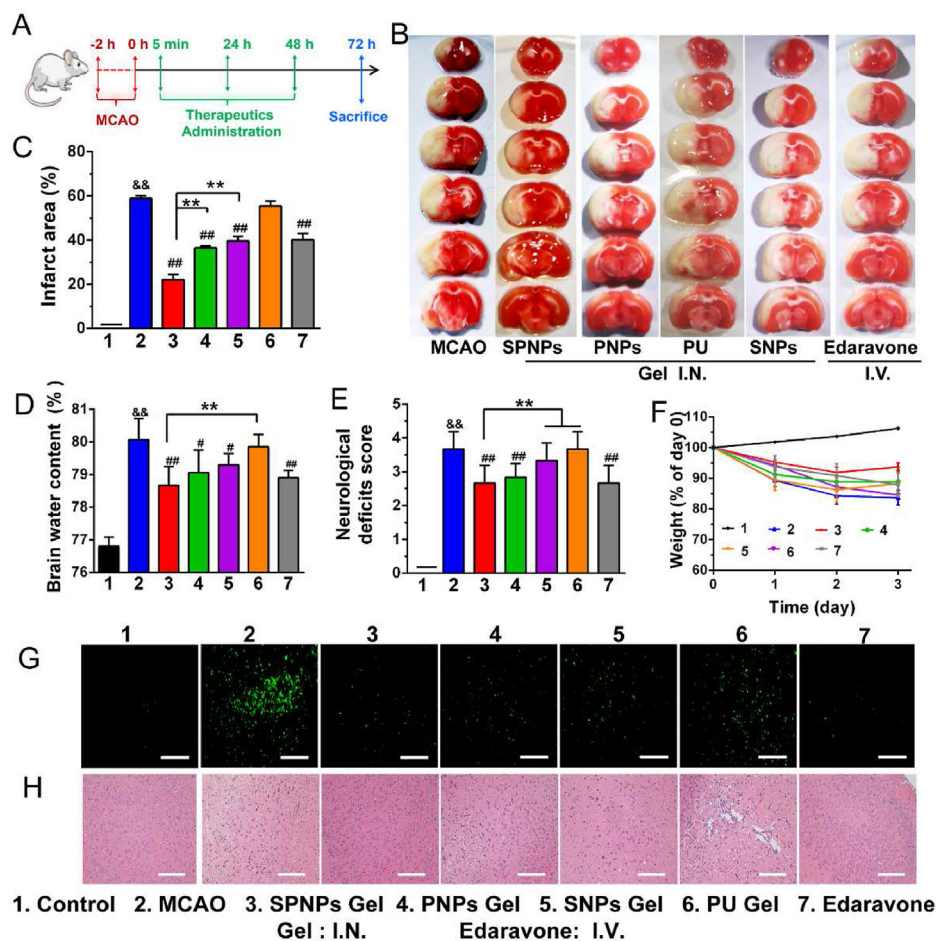


**Figure 5** *In vivo* anti-ischemic stroke efficacy. (A) The time axis of operation of the animal experiment in the MCAO model. (B) Images of TTC staining with different treatments. (C) Quantitative analysis of the ratio of the infarct volume to the total brain volume. (D) Edema volume was evaluated by brain water content and (E) neurological scores of different treatment groups. (F) Rats weight during treatment days. (G) TUNEL and (H) H&E staining of ischemic penumbra sections; scale bar = 100  $\mu$ m. Data are presented as mean  $\pm$  SD ( $n = 5$ ). && $P < 0.01$  vs. control group; or  $###P < 0.01$  vs. MCAO group;  $**P < 0.01$  vs. SPNPs Gel group.

the other treated groups. The SPNPs-gel treatment groups displayed the lowest infarct area of 20%, compared with 38% in the PNP-gel group, or 40% in the SNP-gel group, suggesting the SPNPs-gel had the best protective efficiency. Stroke also led to cerebral edema in rats, and the water content in the ischemic brain hemisphere also was examined (Fig. 5D). Consistent with the results of the infarct area, the water content was reduced in SPNPs-gel with 78.5%, compared to that of 80% in MCAO. The neuro score was further investigated to evaluate the neurological functions of rats. A higher score indicated severe damage. Severe behavioral deficits could be observed in the MCAO model and PU-gel group (Fig. 5E), while the reduced score was displayed in groups with nanoparticles-gels, suggesting their therapeutic efficacy on model rats. The SPNPs-gel demonstrated the lowest score, indicating optimal protection efficacy. Despite the positive efficacy, the rats were weighted to determine the security (Fig. 5F), and no weight loss was seen in treatment groups compared with that in MCAO model rats. While the faster weight loss than the control group was due to the blood loss in establishing the MCAO model.

The apoptosis of nerve cells was studied by TUNEL staining (Fig. 5G), and the intense green fluorescence could be observed in the MCAO group, compared to little fluorescence in the control group. The TUNEL fluorescence intensity decreased in the treatment groups, and the SPNPs-gel treatment demonstrated the weakest fluorescence. Then the H&E staining images were further elucidating the same results. The cells were evenly arranged in the control group, the nuclei were intact and the intercellular spaces were tight (Fig. 5H). However, the cells in the MCAO group proposed significantly larger intercellular spaces, atrophied nuclei, and disordered arrangement, indicating severe edema with damaged cells in the brain tissue after cerebral ischemia-reperfusion. The treatment with different therapeutic agents-gels could alleviate the brain tissue damage, reducing the enlargement of the intercellular space and the shrinkage of the nucleus. The staining data were consistent with the above results, indicating the SPNPs-gel treatment could efficiently alleviate the injury of the stroke brain and achieve anti-ischemic stroke efficacy.

### 3.6. SPNPs against ischemic stroke to reverse neuron damage by alleviating oxidative stress

Multiple factors within the stroke sites were investigated to elaborate on the possible mechanism of reducing ischemic reperfusion injury by SPNPs. Oxidative stress and mitochondrial damage were the typical pathological features after ischemia-reperfusion<sup>4</sup>. Firstly, basic markers such as superoxide dismutase (SOD), malondialdehyde (MDA), and GSH-PX were determined to evaluate oxidative stress at ischemic penumbra (Fig. 6A–C). The ischemic brain damage would induce a decrease of SOD and GSH-PX, or an increase of MDA, which was observed in the MCAO group. The gel treatment groups displayed higher SOD and GSH-PX, and lower MDA levels, compared to the MCAO group. The SNPs gel treatment could recover the SOD, GSH-PX, and MDA levels, indicating the antioxidative effect of ROS-responsive PDAA crosslinker and SS-31. The PU or PNP also showed significant therapeutic effects on reversing oxidative stress. The positive effect of PU and PNP treatment on reversing oxidative stress indicated the therapeutic effect of PU. The synergistic effect on alleviating oxidative stress was elucidated in SPNPs groups with a similar level of SOD, MDA, and GSH-PX as that in the sham group. These data confirmed that the SPNPs

played a role in ROS depletion and subsequent inhibition of lipid peroxidation in the ischemic brain.

The oxidative stress would trigger the initiation of inflammatory damage<sup>33,34</sup>. The intracerebral inflammatory factors levels of TNF- $\alpha$ , IL-1 $\beta$ , and IL-6 were further quantified by ELISA kits (Fig. 6D–F). The production of proinflammatory factors TNF- $\alpha$ , IL-1 $\beta$ , and IL-6 was increased in the MCAO model compared to the sham group. While ROS-depletion of SNPs and anti-oxidation of PU would decrease the TNF- $\alpha$ , IL-1 $\beta$ , and IL-6 levels. Importantly, the SPNPs group exerted a similar expression of TNF- $\alpha$ , IL-1 $\beta$ , and IL-6 as the sham group, affirming the synergistic effect on alleviating oxidative stress. These data manifested that the SPNPs could alleviate oxidative stress and inhibit inflammation in the ischemic microenvironment.

### 3.7. SPNPs restore mitochondrial energy metabolism and morphology after cerebral ischemia/reperfusion injury

Neurons are particularly dependent on mitochondria for calcium buffering and ATP production, and their viability was highly susceptible to mitochondrial defects<sup>17,35</sup>. Mitochondrial damage was inevitable after ischemia-reperfusion, so maintaining mitochondrial function is critical to reversing ischemic damage. During metabolic distress, multiple pathological pathways are activated in mitochondria, including a decrease of ATP production, and dysfunction of sodium-potassium pumps<sup>17,36</sup>.

Maintaining energy dynamics in ischemic penumbra was attractive for stroke therapy. The ATP level was first evaluated (Fig. 6G). The ATP level was significantly reduced in the MCAO group. While an increase of ATP level was observed in therapeutic agents treated rats. And the samples from SPNPs-gel-treated groups demonstrated the level of ATP at 50 mmol/mg protein, which was higher than that at the positive control Edaravone groups. These data indicated that the SPNPs treatment could repair energy metabolism in the ischemic brain. Then the sodium-potassium pumps (Na<sup>+</sup>-K<sup>+</sup>-ATPase pumps) and calcium pumps (Ca<sup>2+</sup>-Mg<sup>2+</sup>-ATPase pumps) on the cell surface would be rescued by the rescued energy metabolism. The activities of Na<sup>+</sup>-K<sup>+</sup>-ATPase (Fig. 6H) and Ca<sup>2+</sup>-Mg<sup>2+</sup>-ATPase (Fig. 6I) were subsequently investigated. Compared with the decreased activity of ATPase in the MCAO model, treated groups with intranasal administration of nanoparticles-gels demonstrated elevated ATPase activity, and the increase was most pronounced in SPNPs-gels. These results in all demonstrated that the SPNPs could rescue ATP generation, and further maintain the function of ion pumps.

To investigate the neuroprotective effect of SPNPs on mitochondria, the mitochondrial morphology was observed by TEM (Fig. 6J)<sup>35,36</sup>. In the control group, the mitochondria appeared to have normal morphology, demonstrating no evidence of swelling, outer membrane breaks, or intracristal dilation. In contrast, a marked mitochondrial ultrastructural injury was apparent in the MCAO group, such as loss or damage of mitochondrial cristae, the appearance of multiple focal vacuoles in the matrix, swelling, and membrane rupture of mitochondria. The samples treated with therapeutic agents could alleviate the damage to the mitochondrial structure by reducing the swelling of mitochondria in neurons of the cerebral ischemic penumbra and repairing mitochondrial ridges. The cells treated with SPNPs and PNP demonstrated normal mitochondrial morphology. While, SPNPs-gel and Edaravone-treated ischemic brain tissue samples had the least number of damaged mitochondria, the normal structure of

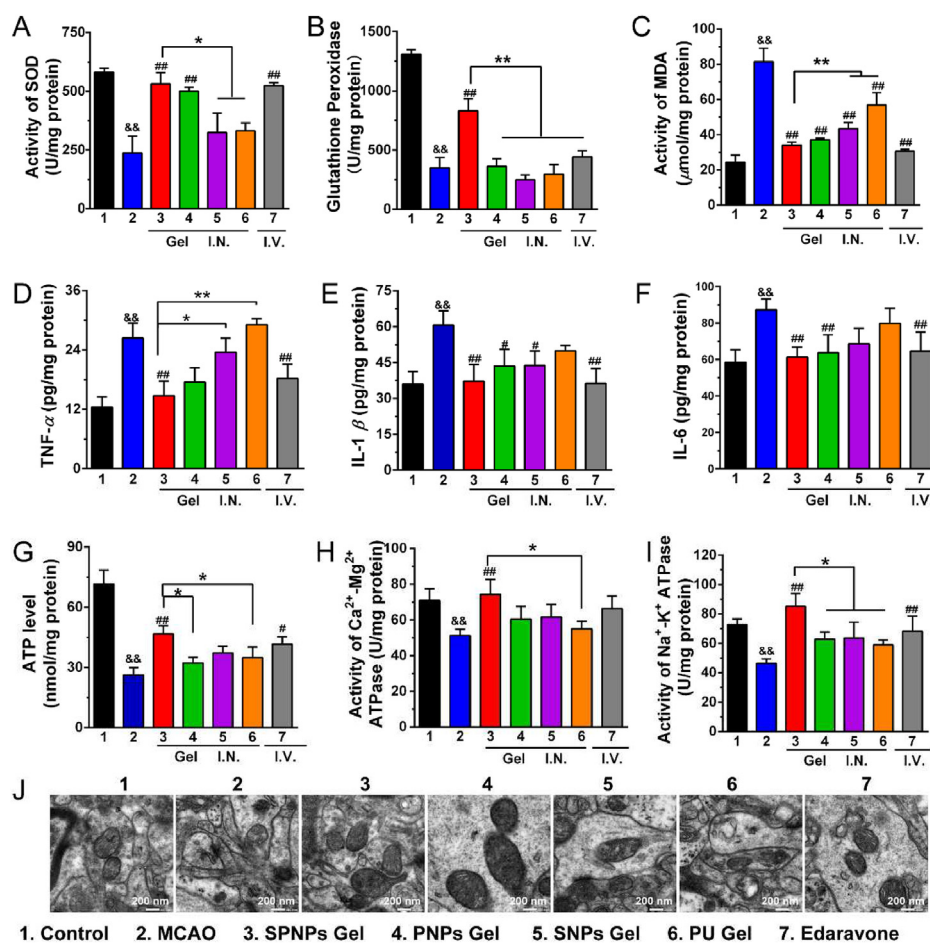


**Figure 6** Mechanism of SPNPs against ischemic stroke to reverse neuron damage. The expression of oxidative stress index as (A) SOD, (B) Glutathione Peroxidase, and (C) MDA in brain tissue after cerebral ischemic-reperfusion. The production of inflammatory factors as (D) TNF- $\alpha$ , (E) IL-1  $\beta$ , and (F) IL-6 in the ischemic hemisphere. The activities of (G) ATP, (H) Ca<sup>2+</sup>-Mg<sup>2+</sup>-ATPase, and (I) Na<sup>+</sup>-K<sup>+</sup>-ATPase in brain tissue. (J) Transmission electron microscope images of neuron mitochondria from the ischemic brain, scale bar = 200 nm. Data are presented as mean  $\pm$  SD ( $n = 5$ ). <sup>&&</sup> $P < 0.01$  vs. control group; <sup>#</sup> $P < 0.05$  or <sup>##</sup> $P < 0.01$  vs. MCAO group; <sup>\*</sup> $P < 0.05$  or <sup>\*\*</sup> $P < 0.01$  vs. SPNPs Gel group.

mitochondrial cristae could be observed under the electron microscope, which was similar to the morphology in the control group. These data show that after cerebral ischemia-reperfusion injury, SPNPs could effectively remodel the mitochondrial ultrastructure with intact membrane morphology.

### 3.8. SPNPs inhibit cerebral ischemia/reperfusion injury-induced neuronal apoptosis

After ischemic stroke, increased oxidative stress induced the open of the mitochondria permeability transition pore (mPTP), and leakage of cytochrome *c* into the cytoplasm, leading to the activation of the apoptosome and caspase-mediated apoptosis<sup>4,37</sup>. To evaluate the effect of SPNPs on mitochondria-mediated apoptosis, the Cytochrome C (CYT C) level in cellular plasma was determined by western blotting (Fig. 7A and B). Compared to the control group, an increased expression of cytochrome *c* protein was observed after ischemic stroke in MCAO, indicating the release of CYT C from mitochondria to the cytosol. Whereas, this expression of CYT C was significantly inhibited after therapeutic nanoparticle treatment. Furthermore, the CYT C levels in the SPNPs group were lowest, indicating the optimal inhibition of mitochondrial permeability.

As a central player in the regulation of apoptosis, the BCL-2 protein family could regulate apoptosis by the control of mitochondrial permeability<sup>4,38,39</sup>. The pro-apoptotic protein (BAX) and anti-apoptotic proteins (BCL-2, and BCL-XL) in the ischemic brain were measured by western blotting and real-time RT-PCR. The expression of anti-apoptotic proteins (BCL-2, and BCL-XL) was downregulated, while the pro-apoptotic protein (BAX) was upregulated due to cerebral ischemia-reperfusion injury (Fig. 7C–F, and Supporting Information Fig. S18). However, intranasal administration of SPNPs could significantly increase the expression of anti-apoptotic proteins and decrease that of pro-apoptotic protein (BAX). The messenger RNA (mRNA) expression level (Fig. 7G–J) also elucidated similar gene expression of the BCL-2 protein family and *Caspase 3*. Compared to MCAO, the administration of SPNPs markedly elevated anti-apoptotic *Bcl-2* and *Bcl-xL* mRNA levels and downregulated pro-apoptotic *Bax* and *Caspase 3* mRNA levels. The protein expression of *Caspase 3* in the ischemic brain was further observed by immunohistochemistry (Fig. 7K). Compared with the control group, the number of brown positive cells in the MCAO group increased significantly, which indicated that the protein expression of *Caspase-3* in the cerebral cortex increased after cerebral ischemia-reperfusion. While in therapeutic agents gel groups, the number of *Caspase-3*-positive

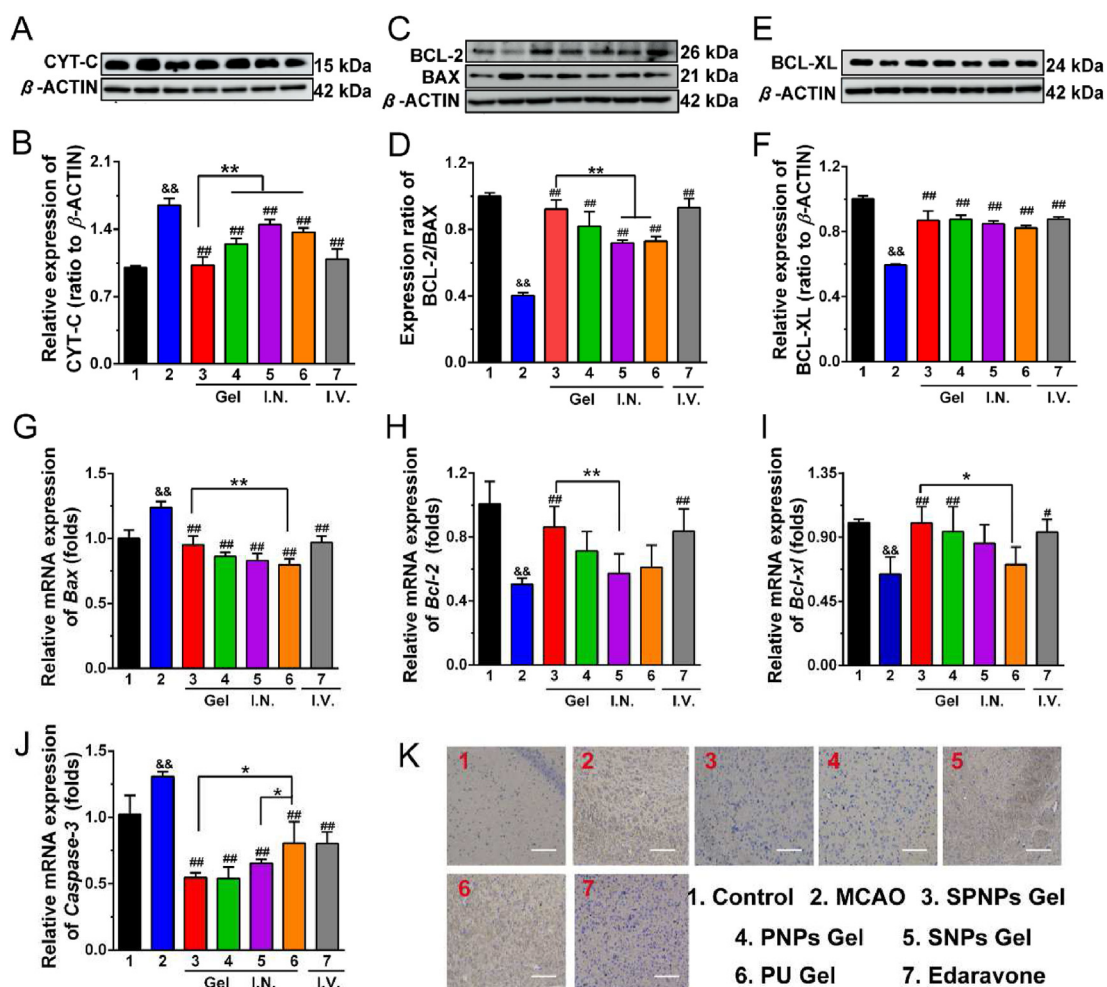


**Figure 7** Apoptosis inhibition is mediated by the inactivation of the mitochondrial pathway. Western blotting analysis of the expression of (A) cytochrome *c* (CYT C), BCL-2 protein family related protein (C) BAX and BCL-2, and (E) BCL-XL in the ischemic hemisphere. Quantitative analysis of changes in the protein levels of (B) cytochrome *c* (CYT-C), (D) BCL-2/BAX ratio, and (F) BCL-XL. Quantitative analysis of changes in the mRNA levels of (G) *Bax*, (H) *Bcl-2*, (I) *Bcl-xl*, and (J) *Caspase 3*. (K) The expression of Caspase 3-positive cells in the ischemic brain by immunohistochemistry, scale bar = 100  $\mu$ m. Data are presented as mean  $\pm$  SD ( $n = 3$ ), <sup>&&</sup> $P < 0.01$  vs. control group, <sup>#</sup> $P < 0.05$  or <sup>##</sup> $P < 0.01$  vs. MCAO group; <sup>\*</sup> $P < 0.05$  or <sup>\*\*</sup> $P < 0.01$  vs. SPNPs Gel group.

cells in the cerebral cortex was significantly decreased. Of note, the Caspase-3-positive cells in SPNPs gel were the least, indicating that SPNPs gel could exert a neuroprotective effect by inhibiting the expression of Caspase-3 cell apoptosis protein. Overall, the SPNPs exerted beneficial effects on neuroprotection by maintaining the integrity and permeability of the mitochondrial membrane, thereby reducing the release of Cytochrome *c* to inhibit the trigger of apoptosis.

#### 4. Conclusions

In summary, multifunctional nanoparticle SPNPs with ROS-responsiveness and mitochondrial-targeted were established for ischemic stroke. The skeleton of nanoparticles was responsive to ROS, consuming intracellular ROS. Mitochondrial targeting SS-31 peptide and ROS-responsive released PU could serve as antioxidants to consume ROS in the mitochondria, maintaining mitochondrial functions. All these concerted actions alleviated the oxidative stress and cascaded inflammation to restore mitochondrial function and inhibit-mitochondria-mediated apoptosis of

neurons. The SPNPs loaded in thermosensitive gels could achieve direct brain delivery by nose-to-brain pathway, and the active targeted ability to ischemic penumbra was realized by the decorated SS-31 peptide. *In vitro* evaluation demonstrated that SPNPs could target mitochondria, maintain membrane potential, and exert a protective effect on H<sub>2</sub>O<sub>2</sub>-induced SH-SY5Y cells. *Ex vivo* fluorescence imaging illustrated the active targeted ability to the ischemic site of SPNPs in MCAO rats. The *in vivo* therapeutic efficacy also illustrated that the SPNPs could greatly ameliorate neuro score, decrease infarct volume, and alleviate brain edema in response to the surgical MCAO injury. Additionally, the detailed mechanism of ischemic stroke therapy *via* SPNPs uptake by neurons was further studied. Alleviation of oxidative stress, reduction of inflammation factors, renovation of mitochondrial function, and decrease of neuron apoptosis could be observed after SPNPs treatment. Therefore, it is suggested that SPNPs may be utilized as a potential multifunctional delivery system to enhance stroke treatment. Besides, the fabrication of multifunctional nanoparticles for other brain diseases needs to be investigated in the future.

## Acknowledgments

This work was supported by National Natural Science Foundation (82272154, China), Tianjin Science Fund for Distinguished Young Scholars (22JCJQC00120, China), Natural Science Foundation of Tianjin (The Basic Research Cooperation Special Foundation of Beijing-Tianjin-Hebei Region, H2022205047, 22JCZXJC00060, and E3B33911DF, China), the Fundamental Research Funds for the Central Universities (3332021068, 3332020059, 2019PT320028, and 2021-RC310-005, China), and the CAMS Innovation Fund for Medical Sciences (2021-I2M-1-058, and 2022-I2M-2-003, China).

## Author contributions

Yan Zhang wrote the manuscript. Haiyun Zhang, Meitong Ou, Faquan Zhao, and Zhengping Jiang carried out the experiments and performed data analysis. Lin Mei supervised the project and revised the manuscript, Yuanlu Cui and Qiangsong Wang designed the research, supervised the project and revised the manuscript. All of the authors have read and approved the final manuscript.

## Conflict of interest

The authors declare no competing financial interest.

## Appendix A. Supporting information

Supporting data to this article can be found online at <https://doi.org/10.1016/j.apsb.2023.06.011>.

## References

- Campbell BCV, Khatri PS. *Lancet* 2020;**396**:129–42.
- Mendelson SJ, Prabhakaran S. Diagnosis and management of transient ischemic attack and acute ischemic stroke: a review. *JAMA* 2021;**325**:1088–98.
- Campbell BCV, De Silva DA, Macleod MR, Coutts SB, Schwamm LH, Davis SM, et al. Donnan ischaemic stroke. *Nat Rev Dis Primers* 2019;**5**:71.
- Qin C, Yang S, Chu YH, Zhang H, Pang XW, Chen L, et al. Signaling pathways involved in ischemic stroke: molecular mechanisms and therapeutic interventions. *Signal Transduct Target Ther* 2022;**7**:215.
- Stinear CM, Lang CE, Zeiler S, Byblow WD. Advances and challenges in stroke rehabilitation. *Lancet Neurol* 2020;**19**:348–60.
- Daniele SG, Trummer G, Hossmann KA, Vrselja Z, Benk C, Gobske KT, et al. Brain vulnerability and viability after ischaemia. *Nat Rev Neurosci* 2021;**22**:553–72.
- Correia AC, Monteiro AR, Silva R, Moreira JN, Sousa Lobo JM, Silva AC. Lipid nanoparticles strategies to modify pharmacokinetics of central nervous system targeting drugs: crossing or circumventing the blood–brain barrier (BBB) to manage neurological disorders. *Adv Drug Delivery Rev* 2022;**189**:114485.
- Kong JL, Chu RX, Wang Y. Neuroprotective treatments for ischemic stroke: opportunities for nanotechnology. *Adv Funct Mater* 2022;**32**:2209405.
- Pandit R, Chen LY, Götz J. The blood–brain barrier: physiology and strategies for drug delivery. *Adv Drug Delivery Rev* 2020;**165–166**:1–14.
- Gorenkova N, Osama I, Seib FP, Carswell HVO. *In vivo* evaluation of engineered self-assembling silk fibroin hydrogels after intracerebral injection in a rat stroke model. *ACS Biomater Sci Eng* 2018;**5**:859–69.
- Nance E, Pun SH, Saigal R, Sellers DL. Drug delivery to the central nervous system. *Nat Rev Mater* 2022;**7**:314–31.
- Li YS, Wu HH, Jiang XC, Dong YF, Zheng JJ, Gao JQ. New idea to promote the clinical applications of stem cells or their extracellular vesicles in central nervous system disorders: combining with intranasal delivery. *Acta Pharm Sin B* 2022;**12**:3215–32.
- Awad R, Avital A, Sosnik A. Polymeric nanocarriers for nose-to-brain drug delivery in neurodegenerative diseases and neurodevelopmental disorders. *Acta Pharm Sin B* 2023;**13**:1866–86.
- Yang XT, Chen XC, Lei T, Qin L, Zhou Y, Hu C, et al. The construction of *in vitro* nasal cavity-mimic M-cell model, design of M cell-targeting nanoparticles and evaluation of mucosal vaccination by nasal administration. *Acta Pharm Sin B* 2020;**10**:1094–105.
- Xi JQ, Zhang RF, Wang LM, Xu W, Liang Q, Li JY, et al. A nanozyme-based artificial peroxisome ameliorates hyperuricemia and ischemic stroke. *Adv Funct Mater* 2021;**31**:2007130.
- He XQ, Wang XR, Yang LY, Yang ZH, Yu WQ, Wang YZ, et al. Intelligent lesion blood–brain barrier targeting nano-missiles for Alzheimer's disease treatment by anti-neuroinflammation and neuroprotection. *Acta Pharm Sin B* 2022;**12**:1987–99.
- Tuo QZ, Zhang ST, Lei P. Mechanisms of neuronal cell death in ischemic stroke and their therapeutic implications. *Med Res Rev* 2022;**42**:259–305.
- Li X, Zhang YB, Ren XY, Wang Y, Chen DX, Li Q, et al. Ischemic microenvironment-responsive therapeutics for cardiovascular diseases. *Adv Mater* 2021;**33**:2105348.
- Dave KM, Stolz DB, Venna VR, Quaicoe VA, Maniskas ME, Reynolds MJ, et al. Mitochondria-containing extracellular vesicles (EV) reduce mouse brain infarct sizes and EV/HSP27 protect ischemic brain endothelial cultures. *J Control Release* 2023;**354**:368–93.
- Li C, Zhao ZH, Luo YF, Ning TT, Liu PX, Chen QJ, et al. Macrophage-disguised manganese dioxide nanoparticles for neuroprotection by reducing oxidative stress and modulating inflammatory microenvironment in acute ischemic stroke. *Adv Sci (Weinh)* 2021;**8**:e2101526.
- Tapeinos C, Pandit A. Physical, chemical, and biological structures based on ROS-sensitive moieties that are able to respond to oxidative microenvironments. *Adv Mater (Deerfield Beach, Fla)* 2016;**28**:5553–85.
- Nie Q, Li CW, Wang Y, Hu Y, Pu WD, Zhang QX, et al. Pathologically triggered *in situ* aggregation of nanoparticles for inflammation-targeting amplification and therapeutic potentiation. *Acta Pharm Sin B* 2023;**13**:390–409.
- Rinaldi A, Caraffi R, Grazioli MV, Oddone N, Giardino L, Tosi G, et al. Applications of the ROS-responsive thioketal linker for the production of smart nanomedicines. *Polymers* 2022;**14**:687–706.
- Yamada Y, Satrialdi Hibino M, Sasaki D, Abe J, Harashima H. Power of mitochondrial drug delivery systems to produce innovative nanomedicines. *Adv Drug Delivery Rev* 2020;**154–155**:187–209.
- Cen J, Zhang RF, Zhao TK, Zhang X, Zhang C, Cui J, et al. A water-soluble quercetin conjugate with triple targeting exerts neuron-protective effect on cerebral ischemia by mitophagy activation. *Adv Healthc Mater* 2022;**11**:e2200817.
- Zhang XP, Sun Y, Yang R, Liu B, Liu Y, Yang JH, et al. An injectable mitochondria-targeted nanodrug loaded-hydrogel for restoring mitochondrial function and hierarchically attenuating oxidative stress to reduce myocardial ischemia-reperfusion injury. *Biomaterials* 2022;**287**:121656.
- Tao T, Liu MZ, Chen MY, Luo Y, Wang C, Xu TT, et al. Natural medicine in neuroprotection for ischemic stroke: challenges and prospective. *Pharmacol Ther* 2020;**216**:107695.
- Li ZJ, Fan Y, Huang CX, Liu QL, Huang MH, Chen BJ, et al. Efficacy and safety of puerarin injection on acute heart failure: a systematic review and meta-analysis. *Front Cardiovasc Med* 2022;**9**:934598.
- Yu CC, Du YJ, Li J, Li Y, Wang L, Kong LH, et al. Neuroprotective mechanisms of puerarin in central nervous system diseases: update. *Aging Dis* 2022;**13**:1092–105.

30. Liu Y, Eaton ED, Wills TE, McCann SK, Antonic A, Howells DW. Human ischaemic cascade studies using sh-sy5y cells: a systematic review and meta-analysis. *Transl Stroke Res* 2018;**9**:564–74.
31. Qi XJ, Xu D, Tian ML, Zhou JF, Wang QS, Cui YL. Thermosensitive hydrogel designed for improving the antidepressant activities of genipin via intranasal delivery. *Mater Des* 2021;**206**:109816.
32. Xu D, Lu YR, Kou N, Hu MJ, Wang QS, Cui YL. Intranasal delivery of icariin via a nanogel-thermosensitive hydrogel compound system to improve its antidepressant-like activity. *Int J Pharm* 2020;**586**:119550.
33. Shi K, Tian DC, Li ZG, Ducruet AF, Lawton MT, Shi FD. Global brain inflammation in stroke. *Lancet Neurol* 2019;**18**:1058–66.
34. Letko Khait N, Ho E, Shoichet MS. Wielding the double-edged sword of inflammation: building biomaterial-based strategies for immunomodulation in ischemic stroke treatment. *Adv Funct Mater* 2021;**31**:2010674.
35. Tian HY, Chen XY, Liao J, Yang T, Cheng SW, Mei ZG, et al. Mitochondrial quality control in stroke: from the mechanisms to therapeutic potentials. *J Cell Mol Med* 2022;**26**:1000–12.
36. Lai YX, Lin PQ, Chen ML, Zhang YX, Chen JH, Zheng MW, et al. Restoration of L-OPA1 alleviates acute ischemic stroke injury in rats via inhibiting neuronal apoptosis and preserving mitochondrial function. *Redox Biol* 2020;**34**:101503.
37. Li YX, Sun JY, Wu RX, Bai JR, Hou Y, Zeng Y, et al. Mitochondrial MPTP: a novel target of ethnomedicine for stroke treatment by apoptosis inhibition. *Front Pharmacol* 2020;**11**:352.
38. Czabotar PE, Lessene G, Strasser A, Adams JM. Control of apoptosis by the BCL-2 protein family: implications for physiology and therapy. *Nat Rev Mol Cell Biol* 2014;**15**:49–63.
39. Pemberton JM, Pogmore JP, Andrews DW. Neuronal cell life, death, and axonal degeneration as regulated by the BCL-2 family proteins. *Cell Death Differ* 2021;**28**:108–22.